A fluid–structure interaction model for assessing the safety of flood gate vibrations due to wave impacts

Tieleman, O.C.; Hofland, B.; Tsouvalas, A.; de Almeida , E.; Jonkman, S.N.

DOI
10.1016/j.coastaleng.2021.104007

Publication date
2021

Document Version
Final published version

Published in
Coastal Engineering

Citation (APA)
Tieleman, O. C., Hofland, B., Tsouvalas, A., de Almeida , E., & Jonkman, S. N. (2021). A fluid–structure interaction model for assessing the safety of flood gate vibrations due to wave impacts. *Coastal Engineering*, *170*, 1-17. Article 104007. https://doi.org/10.1016/j.coastaleng.2021.104007

Coastal Engineering 170 (2021) 104007

Contents lists available at ScienceDirect

Coastal Engineering

journal homepage: www.elsevier.com/locate/coastaleng

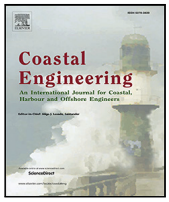

A fluid–structure interaction model for assessing the safety of flood gate vibrations due to wave impacts

O.C. Tieleman *, B. Hofland, A. Tsouvalas, E. de Almeida, S.N. Jonkman

Faculty of Civil Engineering and Geosciences, Delft University of Technology, Stevinweg 1, 2628 CN Delft, The Netherlands

ARTICLE INFO

Keywords:
Flood gate
Vibrations
Wave impacts
Overhang
Fluid–structure interaction
Mode matching
Semi-analytical

ABSTRACT

This paper establishes a computationally efficient model to predict flood gate vibrations due to wave impacts including fluid–structure interaction. In contrast to earlier models, composite fluid domains are included to represent the situation of a flood gate in a dewatering sluice with the presence of an overhang that causes the confined-wave impacts. The dynamic response of the gate-fluid system is derived in the frequency domain using a substructuring mode matching technique, in which the gate vibrations are first expressed in terms of in-vacuo modes while the liquid motion is described as a superposition of linear potentials. Pressure impulse theory is employed to predict the impulsive wave impact loads, which are superposed on the quasi-steady wave loads. The computational efficiency of the developed model allows for a large number of simulations. This makes it possible for the first time to perform probabilistic evaluations for this type of problems without doing concessions on the accuracy of the physical modelling of the involved fluid–structure interaction processes. This is demonstrated by application of the developed models within a probabilistic framework resulting in the explicit quantification of the failure probability of flood gates subjected to wave impacts.

1. Introduction

Flood gates form an essential part of flood defence systems in coastal areas as they regulate the discharge between water bodies and prevent flooding of the hinterland during storm events. These gates are generally subjected to time-varying loads induced by a variety of sources, such as waves, water flow, earthquakes, wind and tides, leading to their dynamic structural response. A key application in which the dynamic behaviour of gates is relevant, is that of flood gates subjected to wave impacts. These impacts generally lead to high peak pressures of short duration (Ramkema, 1978; Hofland et al., 2011; Bagnold, 1939). As part of the flood defence system, gates are required to withstand impact loads with a certain maximum failure probability (Vrijling, 2001).

Several categories of wave impacts on vertical gates can be found in practice: (i) breaking wave impacts due to shoaling, (ii) overtopping wave impacts and (iii) reflecting wave impacts on an overhanging structure (De Almeida and Hofland, 2020). This study focuses on the latter category. Many examples of coastal structures exist where an overhang is present in front of the gate, such as culverts, dewatering sluices with a bridge deck on top and vertical breakwaters with a return crown wall or overhanging slab to reduce overtopping (De Almeida and Hofland, 2020; Kisacik et al., 2014). Violent wave impacts can occur in these situations when reflected standing waves hit the bottom of the overhang in front of the gate. This has for instance been an important design consideration for the renovation of the Afsluitdijk. This dam is located in the Netherlands separating the Lake IJssel from the Waddensea and includes two discharge sluice complexes with flood gates that have an overhang in front (Fig. 1). The presence of an overhang is not only the cause of wave impacts, but additionally affects the hydrodynamic pressures that result from the motion of the gate and therewith the response of the gate-fluid system.

During the lifetime of a flood gate, millions of waves will impact the flood gate. Bagnold (1939) observed that peak pressures accompanied with wave impacts show large variations for waves with very similar characteristics, and are therefore difficult to predict theoretically. A probabilistic approach allows to take into account the uncertainty accompanied with wave impacts. However, probabilistic evaluations require a large number of simulations of the wave impact loads and dynamic analyses.

Within the field of hydraulic engineering, simulating the dynamic response of a structure for a large number of waves or storms is therefore not part of design practice. Within the fields of marine and offshore engineering these type of simulations are more common, for example, when evaluating fatigue damage of offshore platforms (Zheng et al., 2020) or workability of dredging or pipe laying operations (van der Wal and de Boer, 2004). However, simulating the full dynamic behaviour of

* Corresponding author.
E-mail address: o.c.tieleman@tudelft.nl (O.C. Tieleman).

https://doi.org/10.1016/j.coastaleng.2021.104007
Received 14 July 2020; Received in revised form 12 July 2021; Accepted 4 September 2021
Available online 10 September 2021

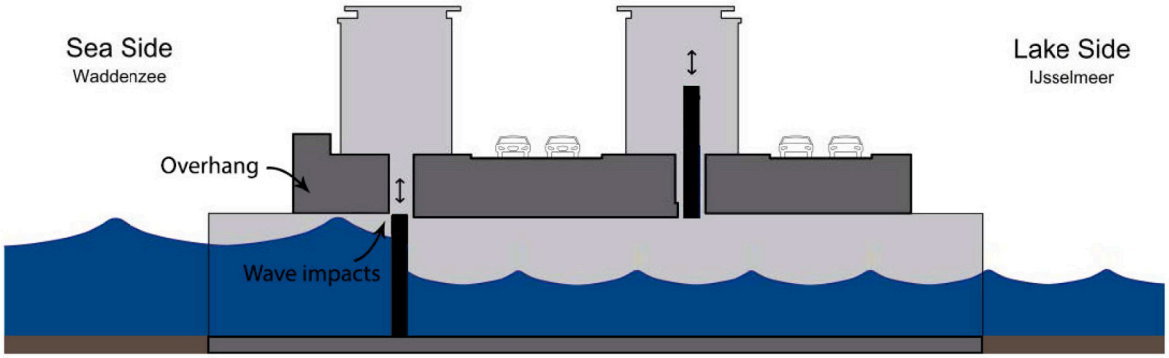

Fig. 1. Impression of an existing flood gate complex in the Afsluitdijk where wave impacts may occur due to the presence of an overhanging structure (De Almeida et al., 2019).

a ship or structure for a multitude of storms to analyse the reliability of the system is also rare within these fields. The main reason for this is the large computational effort necessary to accurately predict the dynamic behaviour of a ship or a structure including the involved fluid–structure interaction for a large number of loads. For a finite element model the time-domain computational task required for a probabilistic evaluation of the dynamic behaviour of a flood gate would be almost an impossible mission given the large number of required simulations (Zheng et al., 2020). Less computationally demanding methods are applied within engineering practice. The most common is a simplified quasi-static approach in which a dynamic amplification factor (DAF) is applied to account for the effect of the vibrations. This factor is derived from a single degree of freedom representation of the structure (Kolkman and Jongeling, 2007a; Cuomo, 2007). The fluid–structure interaction is not explicitly solved but included by using hydrodynamic coefficients. Such an approach lacks the precision to capture the three-dimensional vibration behaviour of a gate-fluid system (Tieleman et al., 2018).

This paper establishes a linear semi-analytical method to predict the dynamic behaviour of a flood gate with an overhang more accurately than the dynamic amplification factor method. The presented method solves the involved fluid–structure interaction in a computationally efficient manner allowing to perform probabilistic evaluations, which is not feasible when applying time-domain finite element methods. This is the first novel contribution of this paper. The method of solution is based on a substructuring mode matching technique similar to Tieleman et al. (2019a) and Tsouvalas and Metrikine (2014). To represent the considered situation with overhang, a solution is derived for composite fluid domains, which was not yet included in earlier models by Tieleman et al. (2019a). The main computational advantage of the mode matching technique lies in the ability to store and reuse partial results in contrast to the stepwise calculation in finite element (FE) methods. For instance, when regarding a large number of loads, the frequency response function of the gate fluid system has to be computed only once. Tsouvalas et al. (2020) have applied this technique to predict the seismic response of liquid storage tanks. Leblond et al. (2009) apply a similar approach for the bending of an elastic cylinder. Three fluid models are considered, namely potential, viscous and acoustic. The modal time dependent displacement coefficients are obtained by matrix inversion in the Laplace domain and fast numerical inversion of the Laplace transform. In Tsouvalas and Metrikine (2016), the mode matching method was successfully employed to predict the noise reduction by the application of an air-bubble curtain in offshore pile driving, showing that a solution can be derived for multiple fluid domains with varying boundary conditions. In this study, the specific solution for the situation of a flood gate with overhang is presented.

The wave impact loads are predicted for a given wave spectrum by employing two separate theories for the quasi-steady and impulsive part of the wave load (De Almeida and Hofland, 2020; Chen et al., 2019). Pressure-impulse theory by Wood and Peregrine (1997) is applied to predict the impulsive wave load. Experiments show that the pressure-impulse is more constant and therefore has a better predictability than the peak pressures (Hofland et al., 2011; Bagnold, 1939; De Almeida and Hofland, 2020). Pressure-impulse theory was recently developed further and validated by Chen et al. (2019) and De Almeida and Hofland (2020). Employing this method to determine the wave impact loads may avoid the necessity for time-consuming and costly physical experiments. This paper presents for the first time the application of this theory in combination with a model to predict the dynamic response of flood gates, in which the latter model includes the responsive fluid pressures resulting from the motion of the gate.

A probabilistic approach is then presented making use of the developed models for the situation of a flood gate subjected to wave impacts due to the presence of an overhang. A Monte Carlo type analysis is performed simulating a large number of storms. Within this approach, the dynamic response of the flood gate is predicted for the consecutive wave impact loads within each storm. In this way, the failure probability of a certain flood gate design can be explicitly determined for given design storm conditions, which is valuable for flood safety assessments. It is a novelty to perform this type of probabilistic evaluations regarding the dynamic response of flood gates, or most other hydraulic structures, without compromising on the accuracy of the physical modelling. The fluid–structure interaction model and probabilistic approach are applied to a case study inspired by the situation of the Afsluitdijk (Rijkswaterstaat, 2020).

The structure of this paper is as follows. The general model approach is discussed in Section 2. The semi-analytical gate-fluid model is presented in Section 3, including a discussion of the model geometry, the theoretical formulation of the problem, the semi-analytical solution and validation by comparison to a finite element model. Subsequently, in Section 4 the approach to predict the wave impact loads is presented. These loads are processed in a probabilistic framework explained in Section 5. In Section 6 the developed models and probabilistic approach are applied to a case study. Finally, results are discussions in Section 7.

2. Overview of the model approach

The developed model within this study consists of several components. The wave impact force on the gate and the gate-fluid response are predicted by separate analytical and semi-analytical models. These models use the same geometry, but different schematisations for the structure and fluid. In this way, the strong points of the different models can be exploited. Fig. 2 gives an overview of the key components of this approach.

In the semi-analytical gate-fluid response model, the wave impact force is modelled as an external excitation force on the gate. This force is assumed not to be altered by the dynamic response of the gate-fluid system. The interaction between the movement of the gate and the pressures in the surrounding fluid is solved within this semi-analytical model using a mode matching technique. The fluid pressures caused by the flexibility of the gate are predicted as part of the response

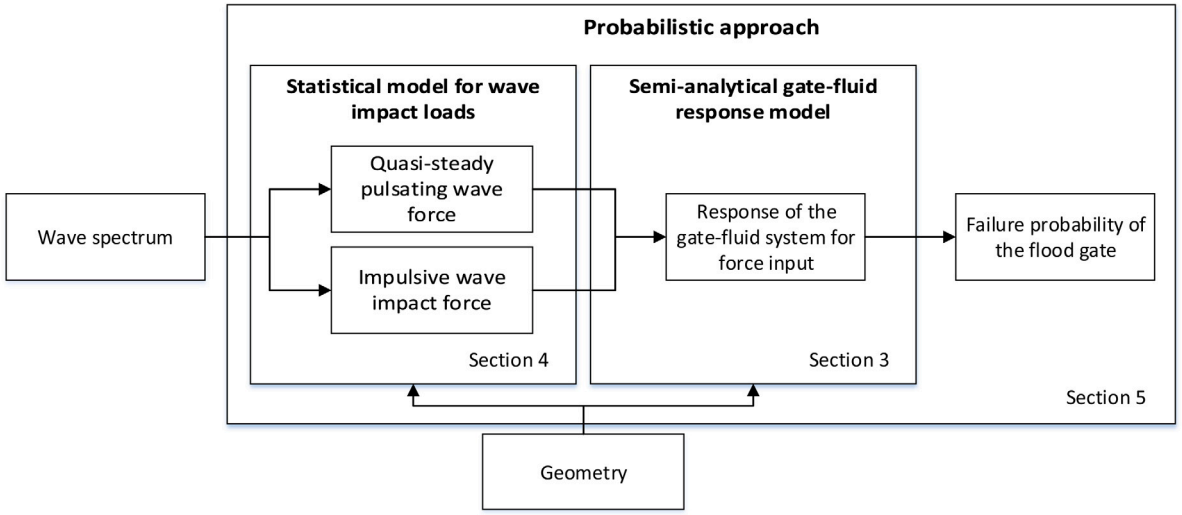

Fig. 2. Overview of the model approach used in this study.

model and effectively superposed on these external wave pressures. In Tieleman et al. (2019a), this was discussed to be a reasonable assumption for the time scales involved in impulsive wave impacts. The validity of this assumption is being tested further in experiments in ongoing studies.

The external wave impact pressures must then be predicted based on a model schematisation with a rigid gate. The wave spectrum is translated to an incoming wave field based on linear wave theory using a statistical approach and translated to wave impact loads. For this purpose, two sub-models are employed. The quasi-steady wave pressure as a result of the pulsating waves is predicted using linear wave theory. Pressure-impulse theory is then applied to predict the wave pressures resulting from the impacts on the overhang. The result is a time-series of the total wave pressure on the gate for a given storm event, which is input to the semi-analytical response model.

The wave impact and response models are both based on linear structural and fluid dynamics in this study. This approach is expected to give a reasonable accuracy for the situation of a gate subjected by wave impact on an overhanging structure, which can be described better by a linear description than for example impacts due to wave breaking. However, it is still the subject of ongoing experiments to what extend phenomena such as the presence of large air pockets under the overhang during the wave impact air entrapment may introduce non-linear behaviour. Because the wave impact pressure is input to the response model in the chosen model approach, one can apply more sophisticated non-linear wave impact models relatively straightforwardly. For the application of the response model to situations with strong non-linear behaviour, the Galerkin method could be employed to approximate the solution.

Both model components are employed within a probabilistic routine to predict the failure probability of the flood gate based on a simulation of its response for a large number of storms. A more extensive overview of this approach and its relation to the underlying models is presented in Section 5.

3. Semi-analytical gate-fluid response model

Section 3.1 gives a description of the gate-fluid model geometry. Section 3.2 then presents the corresponding governing equations that describe the motion of the coupled gate-fluid system. Subsequently, Section 3.3 presents the modal decomposition of the fields. In Section 3.4, the solution to the coupled fluid–structure interaction problem is presented and numerical evaluation is discussed. Finally, in Section 3.5 validation of the developed model is considered.

3.1. Description of the fluid–structure response problem

The geometry of the model is shown in Fig. 3. The gate is represented by a thin flexible plate, which is homogeneous and isotropic and is in full contact with the fluid at the vertical plane. Generally, flood gate designs consist of a front plate and several supporting back beams. More complex gate configurations such as these can be considered straightforwardly by determining the structural modal shapes with existing FE package. However, as this study focuses on correctly representing the hydrodynamic pressures for the presence of an overhanging structure, this relatively straightforward representation of the gate is deemed sufficient without loss of generality.

The gate has a width L_x, height L_z, distributed mass per unit surface ρ_s, and uniform bending rigidity $D = \tilde{E}t^3/(12(1-\nu^2)$, in which $\tilde{E}$ is the modulus of elasticity, t is the thickness of the gate, and ν is the Poisson's ratio. Material damping η is considered by applying a complex modulus of elasticity $\tilde{E} = (1+\eta \mathrm{i})E$ in the frequency domain. The gate is simply supported at its vertical boundaries ($x = 0$, $x = L_x$) and bottom ($z = 0$) while its top edge ($z = L_z$) is stress-free.

Fluid is present in a sluice structure at both sides of the gate, for which three fluid regions can be distinguished. On one side of the gate the sluice has a limited length and an overhang is present. On the other side of the gate the sluice extends to infinity, which is a valid representation of situations with long sluice lengths compared to the water depth. Based on the same method of solution, the model can be extended to include additional fluid domains accounting for a finite sluice length on both sides of the gate.

All regions have impermeable walls and a horizontal bottom. Region I occupies the domain $0 \leq y \leq L_y$ and $0 \leq x \leq L_x^I (= L_x)$. An impermeable overhang is present at $z = L_z$ restricting the fluid flow in the vertical direction. At the moment of a wave impact, the water height h_I in this region is equal to the height of bottom of the overhang. Region II occupies the domain $L_y \leq y \leq \infty$ and $-\Delta x^{II} \leq x \leq L_x^{II} - \Delta x^{II}$. No overhang is present so that the fluid has a free surface. The water level can be equal or higher than in Region I. However, a water level close to the bottom of the overhang generally leads to the highest impact pressures and is thus of most interest (De Almeida and Hofland, 2020). The width of this domain can be chosen much larger than that of Region I to represent the presence of a lake or sea at the end of a sluice or culvert. Finally, Region III occupies the domain $y < 0$ and $0 \leq x \leq L_x^{III} (= L_x)$. This region has similar boundary conditions as Region II. A free surface boundary condition is applied at the free surface. Tieleman et al. (2019b) have presented in which regimes of water depths and excitation frequencies surface waves influence the hydrodynamic response of the structure. Furthermore, the fluid is considered to be compressible, irrotational and inviscid.

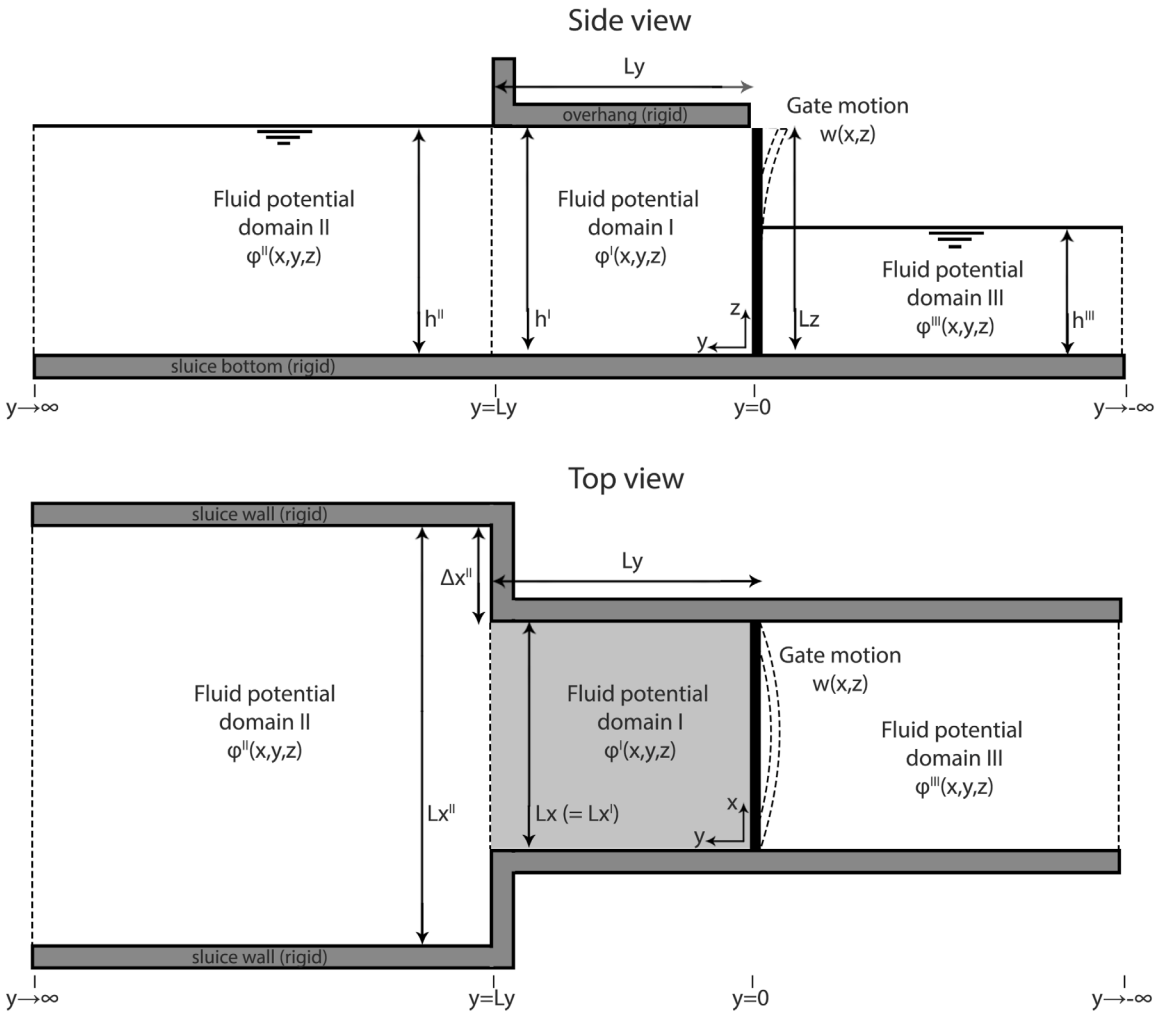

Fig. 3. Side and top view of the model domain consisting of a flexible gate and three fluid regions.

3.2. Governing equations

The governing equations describing the dynamic response of the system are presented. The equation of motion of the gate includes the fluid pressure acting on both sides as well as the external force:

$$\rho_s \frac{\partial^2 w(x,z,t)}{\partial t^2} + D\,\nabla^2\nabla^2 w(x,z,t) = p^I(x,y=0,z,t) - p^{III}(x,y=0,z,t) + f_e(x,z,t) \quad (1)$$

in which w denotes the displacement of the mid-surface of the plate, $\nabla^2 = \frac{\partial^2(\cdot)}{\partial x^2} + \frac{\partial^2(\cdot)}{\partial z^2}$, ρ_s is the distributed mass per unit of area, f_e is the external force, and p_I and p_{III} are the pressures exerted by the fluid on either side. The external force in Eq. (1), being the wave impact force in this study, is predefined. Since the model includes the responsive fluid pressures resulting from the motion of the gate, the external force needs to be based on the situation of a rigid structure. Section 4 presents a theoretical model to predict the wave impact force.

The boundary conditions at $x = 0$; L_z and at $z = 0$; L_z read (Leissa, 1969):

$$w(x=0,z) = M_{xx}(x=0,z) = w(x=L_x,z) = M_{xx}(x=L_x,z) = 0 \quad (2)$$

$$w(x,z=0) = M_{zz}(x,z=0) = M_{zz}(x,z=L_z) = V_{zy}(x,z=L_z) = 0 \quad (3)$$

in which M_{xx} and M_{zz} are the bending moments in x- and z-direction, and V_{zy} is the net shear force in y-direction.

For the description of the fluid motion, the velocity potential function $\phi^j(x,y,z,t)$ is introduced with $j = I, II, III$ denoting the respective fluid region in accordance with Fig. 3. The equation of motion of each fluid region reads:

$$\nabla^2\phi^j(x,y,z,t) - \frac{1}{c_p^{j\,2}}\frac{\partial^2\phi^j(x,y,z,t)}{\partial t^2} = 0 \quad (4)$$

in which c_{pj} is the sound velocity in water in each region. The velocity vector and pressure are given by:

$$\nabla\phi^j(x,y,z,t) = -\mathbf{v}^{\mathbf{j}}(x,y,z,t) \quad (5)$$

$$p^j(x,y,z,t) = -\rho_f^j\frac{\partial\phi(x,z,y,t)}{\partial t} \quad (6)$$

in which ρ_f^j is the fluid density per region. The fluid density in fluid regions I and II will generally be equal. The fluid density at both sides of the flood gate might differ in density however, for example when the flood gate separates sea and fresh water.

Between fluid regions I and II kinematic and dynamic continuity are enforced and at the structure-fluid interfaces velocity compatibility is enforced. This leads to the following interface conditions:

$$\frac{\partial\phi^j(x,y=0,z,t)}{\partial y} = -v_y^j(x,y=0,z,t) = -\frac{\partial w(x,z,t)}{\partial t} \quad (\text{for } j = I, III) \quad (7)$$

$$\rho_f^I\frac{\partial\phi^I(x,y,z,t)}{\partial t}\bigg|_{y=L_y} = \rho_f^I\frac{\partial\phi^{II}(x,y,z,t)}{\partial t}\bigg|_{y=L_y} \quad (8)$$

$$\frac{\partial\phi^I(x,y,z,t)}{\partial y}\bigg|_{y=L_y} = \frac{\partial\phi^{II}(x,y,z,t)}{\partial y}\bigg|_{y=L_y} \quad (9)$$

Furthermore, at $y \to \infty$ and $y \to -\infty$ the radiation conditions should be satisfied at all times in both regions II and III. This results in conditions for the wave numbers in y-direction as discussed further at the end of this section.

The boundary conditions at the impermeable sluice walls and bottom simply state zero fluid velocity. At the still water level of the fluid in regions II and III a pressure release boundary condition is applied, while the overhang poses a zero velocity condition in domain I. This leads to the following boundary conditions:

$$\left.\frac{\partial \phi^j(x,y,z,t)}{\partial x}\right|_{x=0} = \left.\frac{\partial \phi^j(x,y,z,t)}{\partial x}\right|_{x=L_x^j} = 0 \quad (\text{for } j = I, III) \tag{10}$$

$$\left.\frac{\partial \phi^{II}(x,y,z,t)}{\partial x}\right|_{x=-\Delta x^{II}} = \left.\frac{\partial \phi^{II}(x,y,z,t)}{\partial x}\right|_{x=L_x^{II}-\Delta x^{II}} = 0 \tag{11}$$

$$\left.\frac{\partial \phi^I(x,y,z,t)}{\partial z}\right|_{z=0} = \left.\frac{\partial \phi^I(x,y,z,t)}{\partial z}\right|_{z=h^I} = 0 \tag{12}$$

$$\left.\frac{\partial \phi^j(x,y,z,t)}{\partial z}\right|_{z=0} = 0 \quad (\text{for } j = II, III) \tag{13}$$

$$\left.\frac{\partial^2 \phi^j(x,y,z,t)}{\partial t^2}\right|_{z=h_j} + g\left.\frac{\partial \phi^j}{\partial z}\right|_{z=h_j} = 0 \quad (\text{for } j = II, III) \tag{14}$$

Eqs. (1)–(14) complete the mathematical statement of the problem in the time domain.

3.3. Modal decomposition of the fields

By applying the Fourier transform pair as stated below, Eqs. (1)–(14) are transformed to the frequency domain.

$$\tilde{G}(\omega) = \int_{-\infty}^{\infty} g(t)\, e^{-i\omega t}\, dt \tag{15}$$

$$g(t) = \frac{1}{2\pi}\int_{-\infty}^{\infty} \tilde{G}(\omega)\, e^{i\omega t}\, d\omega \tag{16}$$

in which ω is the angular frequency, $g(t)$ is the examined quantity and $\tilde{G}(\omega)$ its amplitude in the frequency domain, i.e. the displacement of the gate or the fluid pressure. A model decomposition scheme is introduced as in Tieleman et al. (2019a) yielding the following modal expansions:

$$\tilde{w}(x,z,\omega) = \sum_{k=1}^{\infty} A_k(\omega)\, W_k(x,z) \tag{17}$$

$$\tilde{\phi}^I(x,y,z,\omega) = \sum_{p=1}^{\infty}\left(B_p^-(\omega)\, e^{-ik_{y,p}^I(L_y-y)} + B_p^+(\omega)\, e^{-ik_{y,p}^I y}\right)\boldsymbol{\Phi}_p^I(x,z) \tag{18}$$

$$\tilde{\phi}^{II}(x,y,z,\omega) = \sum_{r=1}^{\infty} C_r^+(\omega)\, e^{-ik_{y,r}^{II}(y-L_y)}\, \boldsymbol{\Phi}_r^{II}(x,z) \tag{19}$$

$$\tilde{\phi}^{III}(x,y,z,\omega) = \sum_{t=1}^{\infty} D_t^+(\omega)\, e^{-ik_{y,t}^{III}(-y)}\, \boldsymbol{\Phi}_t^{III}(x,z) \tag{20}$$

In Eqs. (17)–(20) local axis systems are introduced for the exponential terms in accordance with Schmidt and Tango (1986) and Jensen et al. (2011) to ensure unconditional numerical stability of the global matrix of equations. The coefficient A_k, B_p^-, B_p^+, C_r^+ and D_t^+ denote the amplitudes (at $y = 0$) of the corresponding plate modes W_k and fluid modes $\boldsymbol{\Phi}_p^I$, $\boldsymbol{\Phi}_r^{II}$ and $\boldsymbol{\Phi}_t^{III}$ in the vertical plane. In region II and III only outgoing waves are permitted to satisfy the conditions at $y = \pm' \infty$.

The wave numbers $k_{y,p}^I$, $k_{y,r}^{II}$ and $k_{y,t}^{III}$ can be found by solving the eigenvalue problem for each region separately (Tieleman et al., 2019a):

$$k_x^{j\,2} + k_y^{j\,2} + k_z^{j\,2} - k_f^2 = 0 \tag{21}$$

A decaying field representing the evanescent waves along the y-direction in region II and III hold for $\mathrm{Im}(k_y^j) \le 0$ while the radiation condition at infinity requires $\mathrm{Re}(k_y^j) \ge 0$ (Tieleman et al., 2019a).

To satisfy Eqs. (10)–(14), the eigenshapes of the fluid in the vertical plane $\boldsymbol{\Phi}_p^I$, $\boldsymbol{\Phi}_r^{II}$ and $\boldsymbol{\Phi}_t^{III}$ are:

$$\boldsymbol{\Phi}_p^I(x,z) = \cos(k_{z,p_1}^I z)\, \cos(k_{x,p_2}^I x)$$

$$\text{with: } k_{x,p_1}^I = \frac{(p_1-1)\pi}{L_x^I} \text{ and } k_{z,p_2}^I = \frac{(p_2-1)\pi}{h^I} \tag{22}$$

$$\boldsymbol{\Phi}_r^{II}(x,z) = \cos(k_{z,r_1}^{II} z)\, \cos(k_{x,r_2}^{II} x)$$

$$\text{with: } k_{x,r_1}^{II} = \frac{(r_1-1)\pi}{L_x^{II}} \text{ and } \omega^2 = -g k_{z,r_2}^{II} \tan\left(k_{z,r_2}^{II} h^{II}\right) \tag{23}$$

$$\boldsymbol{\Phi}_t^{III}(x,z) = \cos(k_{z,t_1}^{III} z)\, \cos(k_{x,t_2}^{III} x)$$

$$\text{with: } k_{x,t_1}^{III} = \frac{(t_1-1)\pi}{L_x^{II}} \text{ and } \omega^2 = -g k_{z,t_2}^{II} \tan\left(k_{z,t_2}^{II} h^{III}\right) \tag{24}$$

The structural modal shapes W_k and corresponding natural frequencies ω_k, which satisfy Eqs. (2)–(3) as well as the unforced equation of motion of the plate, i.e. with zero right-hand side, can be found either analytically or numerically for the presented boundary conditions. Leissa (1969) presents a solution for the boundary conditions used in this study. The only unknowns remaining in Eqs. (17)–(20) are therefore the modal coefficients A_k, B_p^-, B_p^+, C_r^+ and D_t^+.

3.4. Solution to the coupled problem

To solve the coupled problem Eqs. (1)–(14) are transformed to the frequency domain and expanded in terms of Eqs. (17)–(20). By introducing additional sets of structural and fluid modes (e.g. W_l and $\boldsymbol{\Phi}_q^I$) and making use of their orthogonality property in a similar matter as Tsouvalas and Metrikine (2014, 2016) and Tieleman (2016), Tieleman et al. (2019a), the following solvable set of three equations can be derived:

$$\sum_{k=1}^{\infty} A_k\left(I_k\delta_{kl} + \sum_{t=1}^{\infty}\frac{\rho_f\, i\omega^2\, T_{k,t}T_{l,t}}{k_{y,t}\Delta_t}\right) + \sum_{p=1}^{\infty} B_p^-\left(\rho_f\, i\omega\, Q_{l,p}\, e^{-ik_{y,p}^I L_y}\right) + \sum_{p=1}^{\infty} B_p^+\left(\rho_f\, i\omega\, Q_{l,p}\right) = F_l \tag{25}$$

$$\sum_{k=1}^{\infty} A_k\left(\omega\, Q_{k,q}\right) + \sum_{p=1}^{\infty} B_p^-\left(k_{y,p}^I e^{-ik_{y,p}^I L_y}\Delta_q\delta_{pq}\right) - \sum_{p=1}^{\infty} B_p^+\left(k_{y,p}^I\Delta_q\delta_{pq}\right) = 0 \tag{26}$$

$$\sum_{p=1}^{\infty} B_p^-\left(\frac{\rho_f^I}{\rho_f^{II}}\Delta_p\delta_{pq} + k_{y,p}^I\sum_{r=1}^{\infty}\frac{R_{r,q}R_{r,p}}{k_{y,r}^{II}\,\epsilon_r}\right) + \sum_{p=1}^{\infty} B_p^+ e^{-ik_{y,p}^I L_y}\left(\frac{\rho_f^I}{\rho_f^{II}}\Delta_p\delta_{pq} - k_{y,p}^I\sum_{r=1}^{\infty}\frac{R_{r,q}R_{r,p}}{k_{y,r}^{II}\,\epsilon_r}\right) = 0 \tag{27}$$

In above, the modal force is defined as:

$$F_l = \iint_S \tilde{f}_e(x,z)\, W_k(x,z)\, dx\, dz \tag{28}$$

and the impedance coefficients at the two structure-fluid interfaces and the fluid-fluid interface are given by:

$$Q_{l,p} = \iint_S \boldsymbol{\Phi}_p^I(x,z)\, W_l(x,z)\, dx\, dz \tag{29}$$

$$Q_{k,q} = \iint_S \boldsymbol{\Phi}_q^I(x,z)\, W_k(x,z)\, dx\, dz \tag{30}$$

$$T_{l,t} = \iint_S \boldsymbol{\Phi}_t^{III}(x,z)\, W_l(x,z)\, dx\, dz \tag{31}$$

$$T_{k,t} = \iint_S \boldsymbol{\Phi}_t^{III}(x,z)\, W_k(x,z)\, dx\, dz \tag{32}$$

$$R_{r,q} = \iint_{S_w} \boldsymbol{\Phi}_q^I(x,z)\, \boldsymbol{\Phi}_r^{II}(x,z)\, dx\, dz \tag{33}$$

$$R_{r,p} = \iint_{S_w} \boldsymbol{\Phi}_p^I(x,z)\, \boldsymbol{\Phi}_r^{II}(x,z)\, dx\, dz \tag{34}$$

in which S denotes the surface area of the plate. The coefficient I_l is defined as:

$$I_l = \rho_s\,(\omega_l^2 - \omega^2)\, \Gamma_l \tag{35}$$

Finally, Γ_l, Δ_q, Δ_r and Δ_t are the result of the surface integrations of the modes:

$$\Gamma_l = \iint_S W_l^2(x,z)\,dx\,dz \tag{36}$$

$$\Delta_q = \iint_S (\Phi_q^I)^2(x,z)\,dx\,dz \tag{37}$$

$$\Delta_r = \iint_{S_w} (\Phi_r^{II})^2(x,z)\,dx\,dz \tag{38}$$

$$\Delta_t = \iint_S (\Phi_t^{III})^2(x,z)\,dx\,dz \tag{39}$$

By solving this system of equations simultaneously, the unknown sets of coefficients A_k, B_p^- and B_p^+ can be obtained. Subsequently, the coefficients C_r^+ and D_t^+ follow from:

$$C_r = \frac{1}{\mathrm{i}k_{y,r}^{II}\epsilon_r}\sum_{p=1}^{\infty}\left(-B_p^-\,\mathrm{i}k_{y,p}^I + B_p^+\,\mathrm{i}k_{y,p}^I\,e^{-\mathrm{i}k_{y,p}^I L_y}\right)R_{r,p} \tag{40}$$

$$D_t^+ = -\frac{\omega}{k_{y,t}^{III}\Delta_t}\sum_{k=1}^{\infty}A_k T_{k,t} \tag{41}$$

To solve the system of equations, the infinite summations need to be truncated. The amplitude fields of the velocity and pressure at the interfaces between the gate and different fluid domains that result from the solution can be used as a measure of convergence for the number of modes, as discussed in Tsouvalas et al. (2015). In this study, the number of modes is chosen in accordance the standard rules mentioned in Tsouvalas and Metrikine (2016), which means amongst others taking into account all propagating fluid modes. Convergence is subsequently checked by trial and error. Tieleman et al. (2019a) show the convergence for the number of structural modes for a similar problem. Alternatively, one could apply convergence criteria that are based on the satisfaction of the interface conditions between structure and fluid as discussed in Tsouvalas et al. (2015).

The system contains structural damping due to application of a complex modulus of elasticity and fluid damping as a consequence of wave radiation. As a consequence, the solutions for $\tilde{w}$ and v^j will be complex valued. The amplitudes follow from $|w| = \sqrt{\mathrm{Re}(\tilde{w})^2 + \mathrm{Im}(\tilde{w})^2}$ and $|v^j| = \sqrt{\mathrm{Re}(\tilde{v}^j)^2 + \mathrm{Im}(\tilde{v}^j)^2}$. The stresses in the gate follow from the standard strain–stress relations for isotropic homogeneous plates (Leissa, 1969). As a stress criterion Von Mises can be used.

3.5. Validation and performance of the solution

The developed semi-analytical model is validated by comparison with a time-domain finite element model using the standard software package COMSOL (COMSOL Inc, 2018). In Tieleman et al. (2019a) a model was developed and validated for a similar situation as considered in this paper but without an overhang using the same method of solution. The same validation case is therefore used in this study, but now with the addition of an overhang. Both a short and longer overhang will be considered. Table 1 gives an overview of the system parameters for this validation case.

The finite element model in COMSOL is set up for the same geometry. The fluid domains are required to have a finite length in this model. The results show convergence for a domain length of 50 m for both sides of the gate. At the end of the fluid domains a plane wave radiation condition is applied. The model is discretised by a tetrahedral mesh of flexible size between 0.02 and 1 m is applied.

Table 2 shows the resonance frequencies predicted by both the semi-analytical and frequency-domain solver the COMSOL model. The case with the longer overhang results in lower resonance frequencies, as the presence of an overhang leads to an increase in the hydrodynamic mass. The results match closely for both the in vacuo and immersed gate. The in vacuo resonance frequencies and modal shapes of the gate are based on Leissa (1969) and in fact input to the model. The relative difference between this solution and COMSOL is in the order of 1%–2%. The fluid–structure interaction is then solved by the semi-analytical response model to obtain the resonance frequencies of the immersed gate. The predicted resonance frequencies of the immersed gate match even more closely to the outcome of the COMSOL model than for the in vacuo gate. It can therefore be concluded that the developed response model solves the involved fluid–structure interaction with a very minor additional error for this validation case.

An idealised impact force with a triangular temporal variation and a duration of 10^{-3} s is now applied to the gate. Such an impact force of short duration is especially suitable for the purpose of validation, as it ensures a wideband frequency spectrum that excites multiple modes of the system. The response of the case with a long overhang is investigated, as the differences in resonance frequencies predicted by the semi-analytical model and COMSOL were slightly larger for that situation. The time-varying numerical solver of COMSOL is applied to predict the response to the considered impact load. The COMSOL model does not allow for a structural damping coefficient. A distributed damping force of 10^4 Ns/m/m^2 is therefore introduced on the surface of the gate in both models.

Fig. 4 shows the time-domain results of the developed semi-analytical model match closely to the FE model in COMSOL. Minor differences in predicted frequencies of the response do cumulate over time. This has no impact on the magnitude of the response after a single impact, but may have some effect when consecutive impacts within a storm are considered, since ongoing vibrations due to the previous impact can then affect the response to the following impact. However, due to damping this cumulation of frequency differences in the predicted response is limited. Fig. 5 demonstrates this for the case of two consecutive peak loads. The predicted responses by both models match just as closely after the first peak load as after the second peak load. At the end of the considered time window, the difference between the predictions of the semi-analytical and the finite-element model even seem to be smaller than for the single peak load of Fig. 4. Moreover, in this study we present a probabilistic approach in which the random amplitude-phase model is employed to translate the wave spectrum to wave field realisations. In the case that minor phase differences do lead to a higher response after the one wave impact and a lower response after another, this effect will average out over the thousands of storms and waves within each storm considered within this approach. It is therefore expected that this effect has a negligible influence on the outcome of the probabilistic approach presented in this study.

Overall, it can be concluded that the semi-analytical is in very good agreement with the prediction of the time-domain finite element model. However, further validation of the developed model is planned to be performed by comparison with experiments in ongoing studies to investigate effects that are possibly omitted in both models. For the studied validation case, the computation time of the semi-analytical model for the presented time-domain analysis was 36 min on a 3.60 GHz quad core processor, while computation with the COMSOL model lasted approximately 58 h. The computational efficiency of the semi-analytical algorithm has not been fully optimised yet and can still be improved. Furthermore, the semi-analytical model needs only a single computation to obtain the response amplitude operator for a certain frequency range, regardless of the number of loads that is subsequently considered. In contrast, a time-domain FE model needs to compute the response to each different load in order. The semi-analytical model therefore has especially great benefits regarding computational efficiency when a large number of loads is considered. This benefit is employed in the probabilistic approach presented in the next sections.

4. Statistical approach for wave impact loads

A novel approach is employed to predict the impact load on the gate for a certain incoming wave spectrum, i.e. the external force f_e presented in Eq. (1). Within this approach different theories are applied for the quasi-steady pulsating and the impulsive impact part of the wave load resulting in a time-series of the total wave pressure

Table 1
Case parameters and their value.

Structural parameters	Symbol	Value	Unit	Fluid parameters	Symbol	Value	Unit
Width	L_x	12	m	Width	$L_x^{I,II,III}$	12	m
Height	L_z	7.5	m	Water level left	$h^{I,II}$	7	m
Gate thickness	t	0.243	m	Water level right	h^{III}	4	m
Bending stiffness	D	$2.63 \cdot 10^8$	Nm^2	Overhang length	L_y	0.5–5	m
Distributed mass	ρ_s	95	kg/m^2	Fluid density	$\rho_f^{I,II,III}$	1025	kg/m^3
Poisson's ratio (steel)	ν	0.3	–	Fluid sound velocity	c_p	1500	m/s
				Gravitational constant	g	9.81	m/s^2

Table 2
Comparison of the first five predicted resonance frequency predicted by the semi-analytical and COMSOL model for the in vacuo and immersed gate for overhang lengths of 0.5 and 5 m.

Condition	Model	f_1	f_2	f_3	f_4	f_5
In vacuo	Semi-analytical [Hz]	26.1	81.2	97.0	159.6	171.5
	COMSOL [Hz]	25.9	80.6	96.0	157.1	169.1
	Relative difference [-]	0.44%	0.75%	1.04%	1.62%	1.39%
Immersed ($L_y = 0.5$ m)	Semi-analytical [Hz]	5.24	17.8	22.0	39.2	40.2
	COMSOL [Hz]	5.26	17.8	22.0	39.1	39.8
	Relative difference [-]	0.47%	0.04%	0.02%	0.26%	1.01%
Immersed ($L_y = 5$ m)	Semi-analytical [Hz]	3.54	15.0	19.8	34.8	36.8
	COMSOL [Hz]	3.53	15.1	20.0	35.4	37.3
	Relative difference [-]	0.23%	0.6%	1.06%	1.51%	1.34%

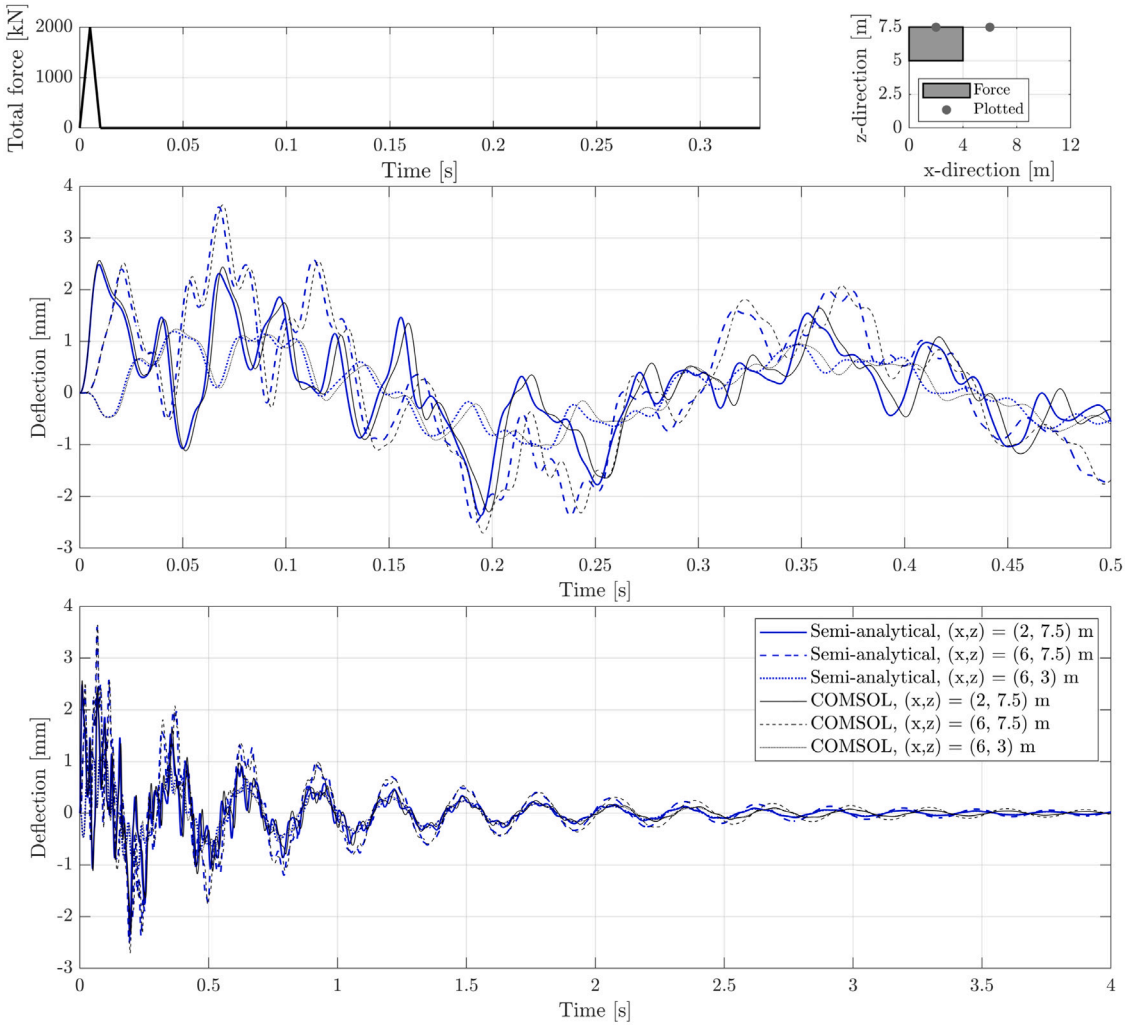

Fig. 4. The time-domain response of the gate immersed in fluid for a triangular peak load predicted by the developed semi-analytical model compared to the FE COMSOL model on two different time scales. The upper right graph shows an overview of where on the surface of the gate the force is applied and of the locations for which the response has been shown.

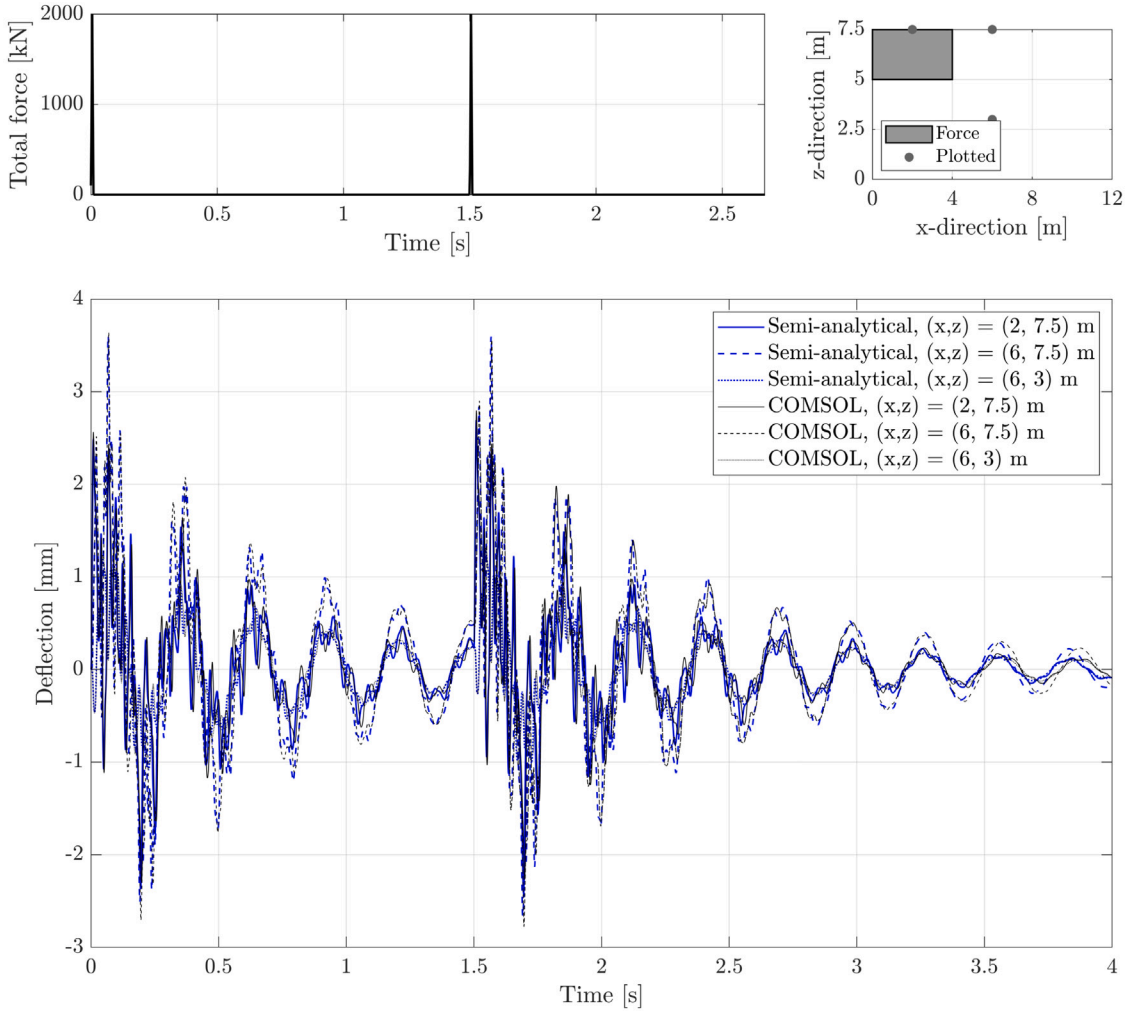

Fig. 5. The time-domain response of the gate immersed in fluid for two consecutive peak triangular loads predicted by the developed semi-analytical model compared to the FE COMSOL model.

on the gate. This approach was recently validated by De Almeida and Hofland (2020) and Chen et al. (2019). Using this method to determine the wave impact loads, the necessity for time-consuming and costly physical experiments can be avoided. Section 4.1 explains the translation from design spectrum to surface elevation. Subsequently, Section 4.2 presents the method to predict the wave load.

4.1. Design wave spectrum

In engineering practice, the most common design spectrum for wind sea in oceanic waters is the JONSWAP spectrum (Hasselmann, 1973). A one-directional JONSWAP spectrum is considered with a design significant wave height H_{m0}.

Linear wave theory is used to obtain the surface elevation and quasi-steady wave force from the wave spectrum. The presented approach does allow for more advanced wave theories, as the developed gate-fluid response model does not require linear force input. Although the response model is based on linear dynamics, any external force may be applied on the gate after applying a Fourier transform to translate it to the frequency-domain. However, in this study linear wave theory is deemed sufficient for the purpose of demonstrating the probabilistic framework. De Almeida and Hofland (2020) have also shown that linear wave theory can be used to predict wave impact loads with reasonable accuracy for a wave steepness up to 2%. Based on the random-phase/amplitude model, a random realisation is generated for the time-record of the surface elevation as the sum of a large number of statistically independent harmonic wave components for the entire duration of the design storm speak (T_{storm}) (Holthuijsen, 2007):

$$\eta_w(y,t) = \sum_{i=1}^{N} a_i \cos(\omega_{w,i} t + k_{w,i}\, y + \phi_i) \tag{42}$$

in which η_w is the surface elevation due to the incoming wave field, a_i is the amplitude of the respective harmonic, following from the energy in the spectrum at the given frequency (band) and $k_{w,i}$ is the wave number following from the dispersion equation for free surface waves $\omega_{w,i}^2 = k_{w,i}\, g \tanh(k_{w,i} h^I)$. The random phase shift ϕ_i is uniformly distributed between 0 and 2π.

The surface elevation at the end of the overhang follows from:

$$\eta_{\text{overhang}}(t) = (1 + c_r)\, \eta_w(y = L_y, t) \tag{43}$$

in which c_r is the reflection coefficient. For the considered geometry with vertical wall, experiments show the reflection coefficient to be close to 1.0. (De Almeida and Hofland, 2020)

4.2. Wave impact loads

Different theories are applied to predict the quasi-steady pulsating and the impulsive part of the wave load for the obtained surface elevation field, such that the total wave pressure is the summation of both (De Almeida and Hofland, 2020; Chen et al., 2019):

$$f_{\text{w}}(x, y = 0, z, t) = f_{qs}(x, y = 0, z, t) + f_{im}(x, y = 0, z, t) \tag{44}$$

in which f_w is the total wave pressure, f_{qs} is the quasi-steady wave pressure and f_{im} the impulsive wave impact pressure. Regarding the developed gate-fluid model, only the wave pressure at the surface of the gate (at $y = 0$) is needed. Fig. 6 shows the separation in these two parts for a typical wave force time series and Fig. 7 shows examples of the pressure and pressure impulse distribution on the gate at given moments in time.

As discussed in Section 2, the wave force is predicted for the situation with a rigid gate, as the gate fluid model includes the responsive fluid pressures resulting from the motion of the gate. For typical flood gates, the impulsive impact part of the wave load is expected to cause gate vibrations, while the quasi-steady part of the wave load gives a quasi-static structural response. However, this distinction in structural response is not necessary in the presented approach, as the total wave load can be applied in the gate-fluid model.

4.2.1. Pulsating wave force

For the quasi-steady pulsating wave pressure linear wave theory is applied, which was recently validated for waves with a steepness up to 3.8% in (De Almeida et al., 2019). The pressure over the vertical up to the bottom of the overhang (i.e. over height of the gate) acting on the surface of the gate is based on the surface elevation at the end of the overhang. This premise is valid for a short overhang length (L_y) in comparison to the deep water wave length (L_0), i.e. $L_y/L_0 < 0.1$ (De Almeida and Hofland, 2020). The pressure at the gate then following from the well known relation:

$$f_{qs}(z,t) = \sum_{i=1}^{N} \rho_f^I g\, \eta_{\text{overhang},i}(t)\, \frac{\cosh(k_{w,i} z)}{\cosh(k_{w,i} h)} \tag{45}$$

in which $\eta_{\text{overhang},i}$ is the surface elevation at the end of the overhang caused by each individual random harmonic wave and its reflection ($\eta_{\text{overhang},i}(t) = (1 + c_r)\eta_{w,i}(y = L_y, t)$). Higher-order theories or Goda could be used for waves of higher steepness.

4.2.2. Impulsive wave force

At the moment the upward moving wave surface hits the bottom of the overhang a violent wave impact occurs (De Almeida and Hofland, 2020). Bagnold (1939) observed that peak pressures accompanied with wave impacts show large variations for waves with very similar characteristics, and are therefore difficult to predict theoretically. However, as discussed in Hofland et al. (2011) and De Almeida and Hofland (2020), the pressure-impulse shows to be remarkably constant and therefore has a better predictability. For this reason, pressure-impulse theory is applied in this study to predict the impulsive wave force. The pressure-impulse is defined as the area enclosed by the pressure–time curve:

$$P_{im}(x,z) = \int_{t_0}^{t_1} f_{im}(x,z,t) \tag{46}$$

in which t_0 and t_1 define the start and end of the impact peak respectively.

The theory of Wood and Peregrine (1997) is used to predict the pressure impulse field as a function of the upward wave velocity at the moment of impact. This method assumes governing equations as shown in Fig. 7, excluding both the effect of free surface waves and compressibility on the pressure impulse. The dimensionless pressure impulse of a wave impact is defined as: (De Almeida and Hofland, 2020):

$$\bar{P}(x,y,z) = \frac{P(x, y = 0, z)}{\beta_{im}\, \rho_f^I U_w L_y} \tag{47}$$

in which P is the pressure impulse, β_{im} a correction factor for the effect of compressibility of entrapped air, U_w is the impact velocity of the considered wave impact and L_y is the overhang length. The pressure impulse is regarded at the surface of the flood gate ($y = 0$).

The dimensionless pressure impulse field (i.e. $\bar{P}$) is constant for a given geometry and can be solved numerically. For the situation with an overhang, Wood and Peregrine (1997) have also presented a semi-analytical solution. Fig. 8 shows the dimensionless pressure impulse shape over the depth for several water depth over overhang length ratios. For a further description of this solution, is referred to Wood and Peregrine (1997) and De Almeida and Hofland (2020).

The magnitude of the pressure impulse depends on the impact velocity of each wave impact, which is the upward velocity of the waterfront at the moment of impact. This velocity is known for each impact from the surface elevation time-series. For this purpose, again the surface elevation at the end of the overhang is considered. The moment of impact happens at each upward crossing of the level of the overhang bottom, i.e. when $h^I + \eta_{\text{overhang}}(t) = L_z$.

In experiments De Almeida and Hofland (2020), de Almeida and Hofland (2020) have shown that the compressibility of entrapped air between the overhang and standing wave crest may in practice lead to larger impact impulses than the analytical solution predicts. For this reason, the correction factor β_{Im} is introduced in Eq. (47). Based on experiments, De Almeida and Hofland (2020) derived a value of 1.17 for this correction factor in the case of short overhang lengths ($L_y/h^I \ll 1$). Finally, through the impact peak duration τ the pressure impulse field is translated to a triangularly shaped peak time series of the impact pressure, as shown in Fig. 6. This impulsive pressure is added to the quasi-static pulsating wave pressure resulting in a time-series of the total wave pressure, of which the lower part of Fig. 14 shows an example.

5. Probabilistic approach for wave impacts on a flood gate

The numerical efficiency of the developed gate-fluid and wave load models makes it possible to perform a large number of simulations. This allows to evaluate the structural reliability of the gate. A probabilistic approach is presented to explicitly quantify the failure probability of a flood gate design making use of the developed models, which is valuable for safety assessments and design. Within this approach, a Monte Carlo simulation is performed in which the dynamic behaviour of the gate is evaluated for a large number of storm simulations following from the statistically described design wave spectrum. Fig. 9 shows an overview of the presented probabilistic approach.

The following variables related to the wave loads are considered stochastically:

- The phase shift ϕ_i of each surface elevation harmonic is considered uniformly distributed between 0 and 2π in accordance with the well-known random phase/amplitude model as for instance discussed in Holthuijsen (2007).
- The correction factor β_{Im} to account for the variability of the pressure impulse due the compressibility of entrapped air between the overhang and standing wave crest. The factor is considered normally distributed with a mean $\mu_{\beta_{\text{Im}}} = 1.17$ and standard deviation $\sigma_{\beta_{\text{Im}}} = 0.11$. This distribution has been derived by (De Almeida and Hofland, 2020) based on experiments dedicated to the specific situation of a gate with overhang.
- The wave impact duration τ for each impulsive wave impact. Measurements (De Almeida and Hofland, 2020) show that the impact durations of wave impacts on an overhang vary between 10 to 200 ms independent of the wave characteristics such as impact velocity. Based on those results a triangular distribution is proposed with $a = 0.010$, $b = 0.105$ and $c = 0.200$ s.

The water levels at both sides of the flood gate are considered to be constant during the duration of the storm. On the sea side a water level equal to the bottom of the overhang is considered, which leads to the highest wave impact loads. This assumption is therefore expected to lead to a conservative estimate of the failure probability of the flood gate. The distribution of water levels during the course of the design storm can be included straightforwardly within the presented method.

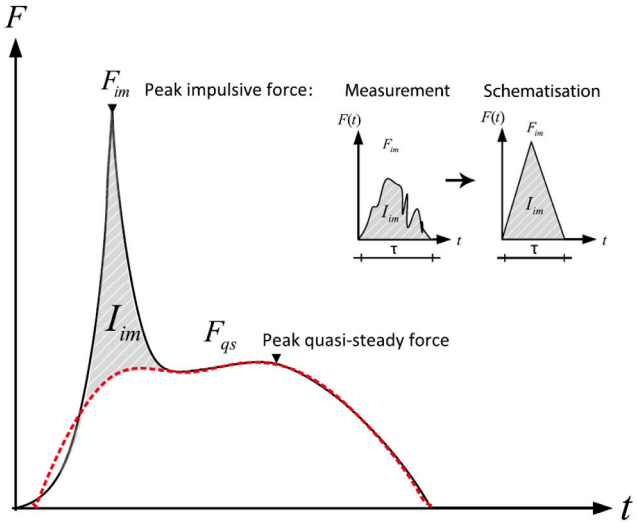

Fig. 6. Typical time history of a wave impact on a (vertical) wall with or without a horizontal overhang split into a quasi-steady and impulsive part. The impulsive load is schematised as a triangular peak with duration τ. (Chen et al., 2019).

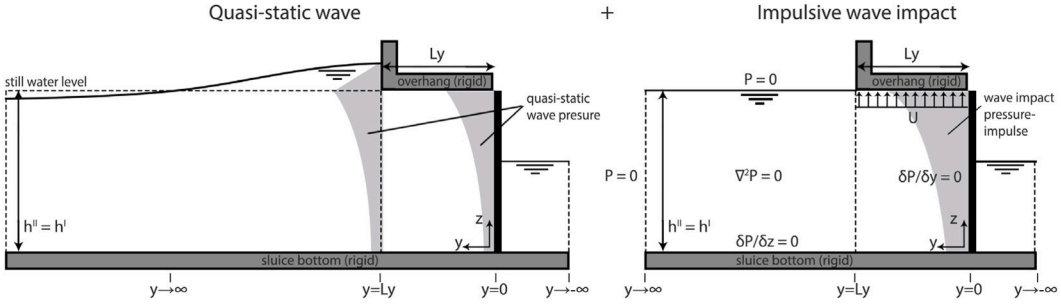

Fig. 7. Example of the quasi-steady wave pressure (at the moment of a wave top) and the wave impact pressure impulse (at the moment of impact) acting on the gate.

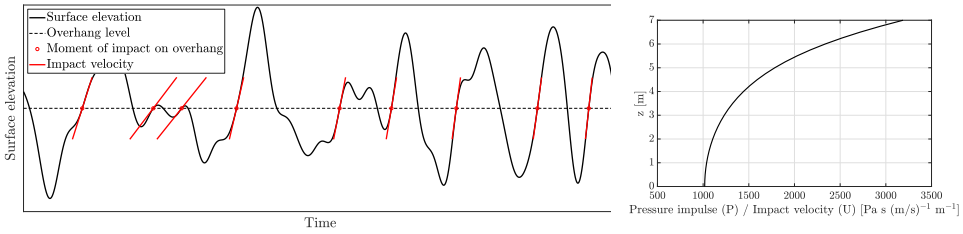

Fig. 8. Example of surface elevation with the moments and velocities of impact (left) and the pressure impulse shape on the gate for varying overhang lengths (right).

A Monte Carlo simulation is performed in which a number of realisations N is generated for the time-series of the wave impact pressures for a given design wave spectrum $S(\omega_p)$ and storm duration T_{storm}. The gate-fluid model is employed to determine the response of the flood gate for each storm realisation. In this study, the parameters of the responsive gate and fluid model are considered deterministic. However, within the given approach stochastic variables can be used for these parameters as well.

As a failure criterion the Von Mises stress is used, which for general plane stress states:

$$\sigma_v = \sqrt{\sigma_{xx}^2 - \sigma_{xx}\sigma_{yy} + \sigma_{yy}^2 + 3\tau_{xy}^2} \leq f_y \tag{48}$$

with f_y being the yield strength of the steel material. The failure probability of the gate the follows from:

$$p_f = \frac{n_{\text{fails}}}{N} \tag{49}$$

in which p_f is the failure probability of the gate, n_{fails} is the number of simulations in which the gate fails and N is the total number of simulations.

6. Case study afsluitdijk

The presented semi-analytical gate-fluid model, wave load theory and probabilistic approach are applied to a case study inspired by the situation of the Afsluitdijk. The Afsluitdijk in the Netherlands separates Lake IJssel from the Waddensea. This dam contains two discharge sluice complexes in which a large number of gates regulate the water discharge and protect the hinterland from flooding during a storm event. The coming years the Afsluitdijk is being renovated, which includes the replacement of the flood gates. In Fig. 1, an impression is shown of a set of gates in one of discharge sluices. The flood gate at the Waddensea side is considered in this case. The flood gate is required to have a maximum failure probability of 0.1 for the design storm. A 1000 design storms with a duration of 4 h are simulated according

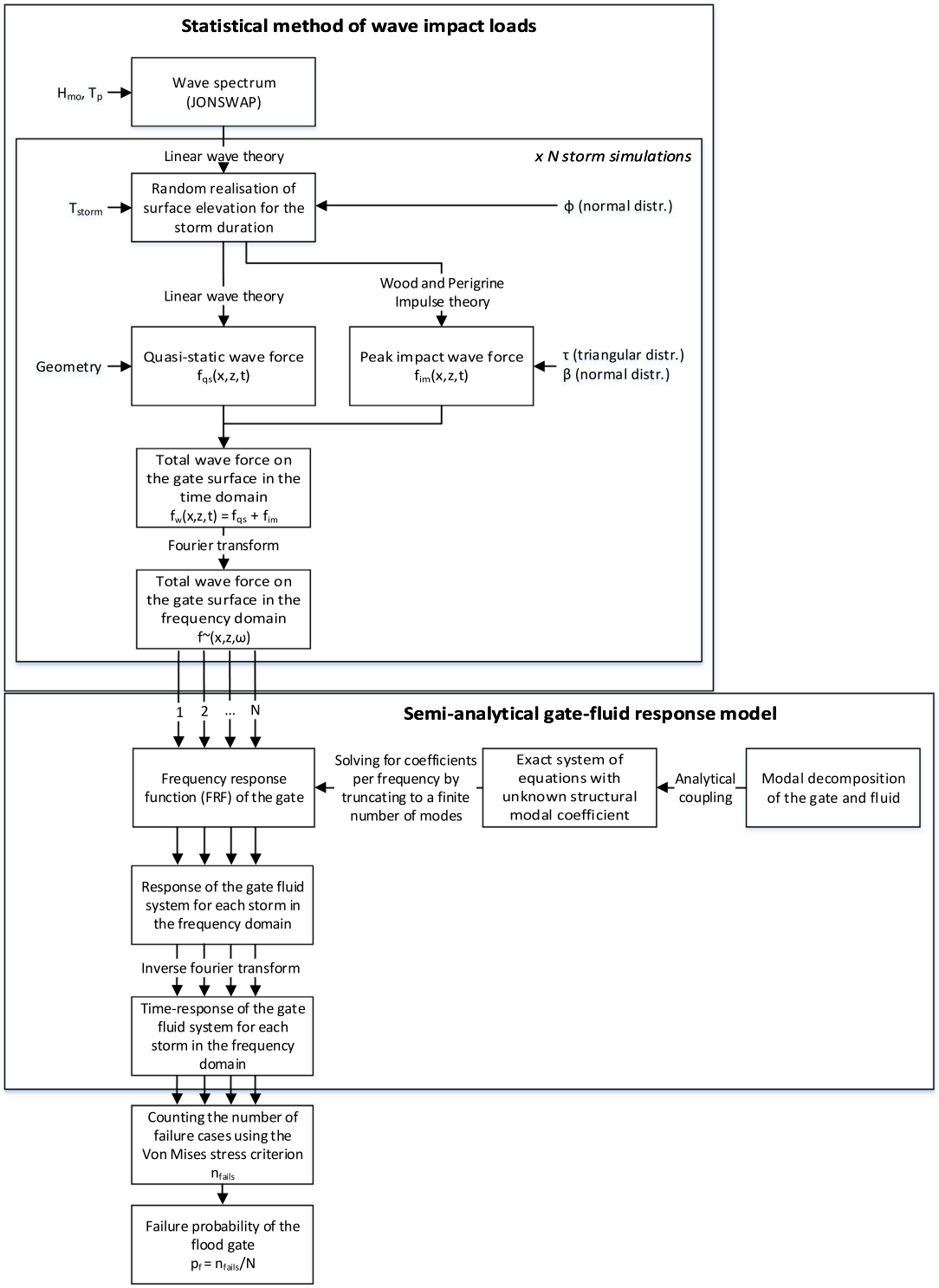

Fig. 9. Overview of the probabilistic approach for the dynamic response of a gate with overhang to wave impact loads.

to the approach presented in previous section to quantify the failure probability of the gate. When less than 100 of the 1000 storms lead to structural stresses exceeding the capacity, this means that the required maximum failure probability is met. The number of simulations in relation to the accuracy of the estimated failure probability will be discussed further on.

In Section 6.1 the parameters of the gate and fluid system are introduced and the resulting resonance frequencies are investigated. Section 6.2 presents the design storm and the resulting incoming wave field and impact loads. Subsequently, in Section 6.3 the dynamic response of the gate fluid system is investigated for a few consecutive wave impacts. Section 6.4 presents the probability of failure of the flood gate by means of a Monte Carlo analysis. Finally, Section 6.5 discusses the accuracy of this analysis in relation to the number of simulations performed.

6.1. Gate-fluid system

Table 3 gives an overview of the relevant case parameters regarding the gate-fluid system. The parameters are in accordance with the model description presented in Section 3.1. High water and waves are present at the Waddensea side of the flood gate. At the other side of the gate low water is present. The sluice length at the Waddensea side of the gate is limited compared to the water depth. A much wider second fluid domain is therefore considered. The sluice length at the lake side of the gate is sufficiently long to be considered infinite with respect to the hydrodynamic pressures acting on the gate.

The approximate resonance frequencies and responses of the gate in vacuo and immersed are obtained by exciting the system by a harmonic load with a range of frequencies. Table 4 shows the first ten resonance frequencies of the gate in vacuo and immersed. These resonance frequencies are all within the range of the peak impact durations, i.e. 10 to 200 ms, and may therefore give a dynamic response. Since in the studied case, the wave impact loads have a constant magnitude over the width of the gate, there will be no response to the modes that are antisymmetric in horizontal direction. For the given water levels, Fig. 10 shows the first four shapes of immersed gate resulting from the semi-analytical model that are not antisymmetric.

Fig. 11 shows the fluid pressure amplitudes for two of the resonance frequencies of the submerged gate. The effect of the boundary condition imposed by the presence of the overhang on the distribution of the fluid pressure can be seen clearly. Furthermore, the fluid pressure shows to be continuous over the interface between fluid domain I and II, satisfying the interface conditions between these two domains.

6.2. Design storm

A design storm with a total duration of four hours is considered in this case study. The water level at the sea side (Waddensea) is considered to be at the overhang level for the entire duration, which is the governing water level in terms of wave impact pressures. However, with the presented methods a multivariate probabilistic analysis including water levels and wave heights could be carried out as well. The wave field is incoming from the sea side of the gate where the high water level is present, and is described by a JONSWAP spectrum with a peak period T_p of 4.5 s and a significant wave H_{m0} of 1.5 m. Table 5 gives an overview of the wave impact parameters and their probabilistic distributions as discussed in Sections 4 and 5 .

The applied spectrum contains relatively steep waves above the limit of 2% for linear theory as mentioned earlier. Higher order wave theory can be applied in design to obtain a more accurate prediction. However, for the purpose of demonstrating the probabilistic framework linear wave theory is deemed sufficient. Moreover, the difference between the free surface velocity predicted by linear and higher order wave theory happens to be minor around the point of the still standing water level, which is considered to be at the overhang level for the entire storm duration in this case study (Tadjbakhsh and Keller, 1960). The impact velocity, which is the governing parameter for the impulsive impact load, is therefore expected to be predicted reasonably by linear wave theory for this case.

As an example, Fig. 12 on the left hand side shows the wave force distributed over the gate width for a one minute time interval of a certain storm realisation using the parameters of Tables 3 and 5. The impulsive impact peaks can be distinguished clearly and show quite some variability in magnitude. On the right hand side, the magnitude of all 3903 peak impacts that occur within this 4 h storm simulation are shown.

Fig. 13 shows the exceedance probability of the maximum wave force distributed over the gate width in a single storm with a duration of 4 h based on the 1000 storm simulations performed in this case study. The maximum wave force found in the performed simulations is approximately 9000 kN/m.

6.3. Response of the gate to several waves

The developed semi-analytical model is now used to determine the response of the gate-fluid system. Fig. 14 shows a time series of the deflection of the gate in response to several consecutive wave impacts. The response is governed by the first resonance mode. However, higher modes are excited by the wave peak impacts of shorter duration, which can be seen especially in the response after the third peak impact (at $t \approx 101$ s).

Vibrations of the gate do not fully damp out between wave impacts. In this case, vibrations from the previous wave impact quite strongly influence the maximum response after the following impact. The sequence and exact moment of wave impacts are therefore relevant when predicting the reliability of the flood gate. This effect is not included in conventional design methods using the dynamic amplification factor (Kolkman and Jongeling, 2007b), but is captured well within the presented probabilistic approach.

Moreover, the maximum peak force does not lead to the maximum response for this time interval. Fig. 15 shows the maximum response of the gate for all wave impacts occurring with a single four hour storm for both the peak force and the pressure impulse of each wave impact. Above a certain limit, higher peak pressures no longer lead to a significant increase in response, most likely because the structural system is insensitive to the short impact durations of those wave impacts. The structural response is therefore more strongly correlated to the pressure impulse than to the peak pressure of a wave impact. This motivates the use of pressure impulse theory as the governing load parameter for wave impacts on these particular type of structures in contrast to the peak force that is often used within design practice. As discussed in Section 4.2.2, the pressure impulse of a wave impact has also shown to be better predictable in experiments (Hofland et al., 2011; De Almeida and Hofland, 2020).

Fig. 15 shows a large variation in the response of the gate for both the peak force and pressure impulse. The previously described effect of consecutive wave impacts is the main cause for this variation. Further, the distribution of the correction factor β_{lm} causes some variation.

Fig. 16 shows the deflection and yield stress fields over the plate for the moment of maximum deflection during the interval considered in Fig. 14.

6.4. Probability of failure of the system

The gate response is now investigated for a thousand storms simulations, determining the maximum stress in the gate for each storm. Exceedance of the yield stress at any time during the four hour storm, is considered as failure of the gate. Fig. 17 shows the maximum stress found in each of the storm simulations and their distribution. The yield stress is exceeded in 25 of the 1000 simulations, leading to the following failure probability of the gate for the given design storm:

$$p_{f,\mathrm{gate}} = \frac{n_{\mathrm{fails}}}{N} = \frac{25}{1000} = 0.025 \tag{50}$$

The failure probability is below the required maximum of 0.1, so that in this case study the gate design suffices.

In the previous analysis, the yield strength was considered as a deterministic value. The probability of failure is also investigated for the situation in which the yield strength of the steel gate is considered stochastically with a mean value 460 N/mm^2 and a standard deviation of 20 N/mm^2. The uncertainty involved with the yield strength of the gate leads to a higher number of failures, resulting in a failure probability of 0.035.

Table 3
Gate-fluid system parameters and their value as applied in the case study.

Structural parameters	Symbol	Value	Unit	Fluid parameters	Symbol	Value	Unit
Width	L_x	12	m	Width domain I	L_x^I	12	m
Height	L_z	7.5	m	Width domain II	L_x^{II}	60	m
Gate thickness	t	0.22	m	Width domain III	L_x^{III}	12	m
Bending stiffness	D	$1.95 \cdot 10^8$	Nm^2	Water level domain I	h^I	7	m
Distributed mass	ρ_s	345	kg/m^2	Water level domain II	h^{II}	7	m
Modulus of elasticity (steel)	E	$200 \cdot 10^9$	Nm^2	Water level domain III	h^{III}	4	m
Moment of inertia	I	0.00089	m^4	Overhang length	L_y	3	m
Poisson's ratio (steel)	ν	0.3	–	Fluid density domain I–III	ρ_f^I	1025	kg/m^3
Yield strength (steel)	f_y	$460 \cdot 10^6$	N/m^2	Fluid sound velocity I–III	c_p^I	1500	m/s
Material damping (steel)	η	0.01	–	Gravitational constant	g	9.81	m/s^2

Table 4
First ten resonance frequencies of the gate in vacuo and immersed.

Condition	f_1	f_2	f_3	f_4	f_5	f_6	f_7	f_8	f_9	f_{10}
In vacuo [Hz]	11.8	36.7	43.8	72.1	77.5	115.2	116.4	134.6	145.2	173.6
Immersed [Hz]	3.5	13.6	16.3	29.1	32.1	50.0	53.5	64.4	66	69.9

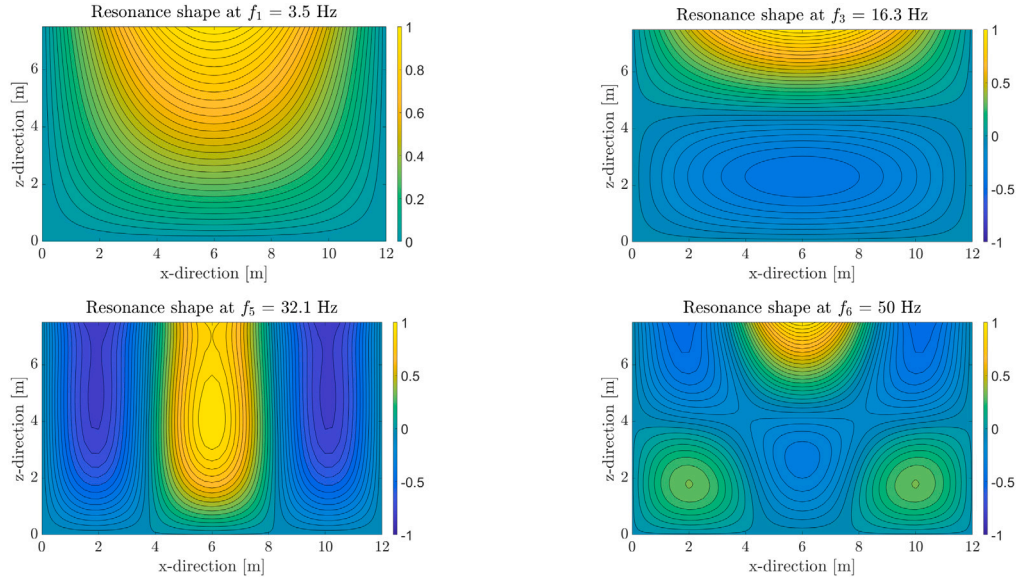

Fig. 10. The amplitude of the complex valued response $|w|$ of the immersed gate for several resonance frequencies.

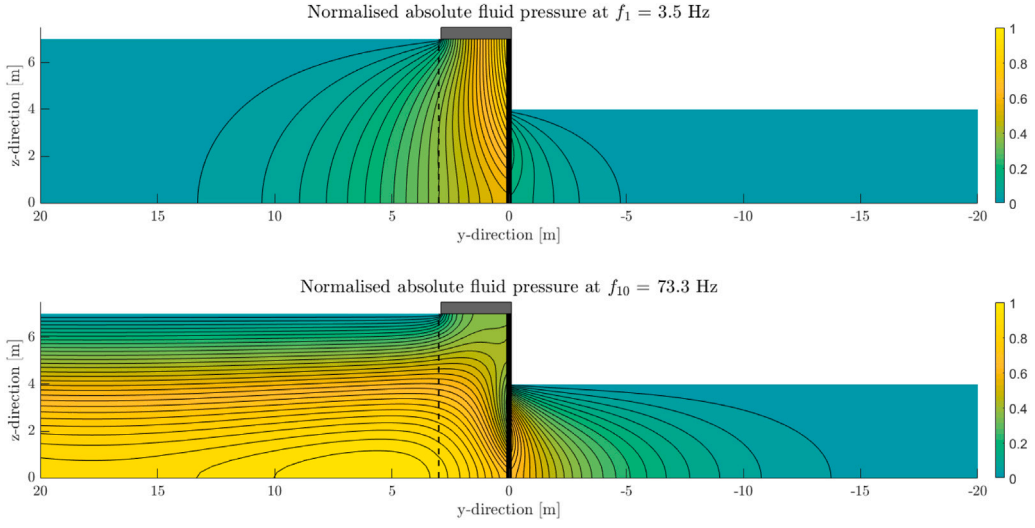

Fig. 11. Normalised absolute fluid pressure at $x = 4$ on both sides of the gate for two resonance frequencies of the immersed gate.

Table 5
Design storm parameters and their distribution and values as applied in the case study.

Parameter	Symbol	Distribution	Value (range)	Unit
Water levels	h^I, h^{II}, h^{III}	Deterministic	(See Table 3)	
Storm duration	T_{storm}	Deterministic	4	hours
Peak period (JONSWAP spectrum)	T_p	Deterministic	4.5	s
Significant wave height (JONSWAP spectrum)	H_{m0}	Deterministic	1.5	m
Reflection coefficient	c_r	Deterministic	0.8	–
Impact peak duration	τ	Triangular	$10 \leq \tau \leq 200$	ms
Surface elevation phase shift (per harmonic i)	ϕ_i	Uniform	$0 \leq \phi \leq 2\pi$	rad
Impulse correction factor	β_{im}	Normal	$\mu_\beta = 1.17$, $\sigma_\beta = 0.11$	–

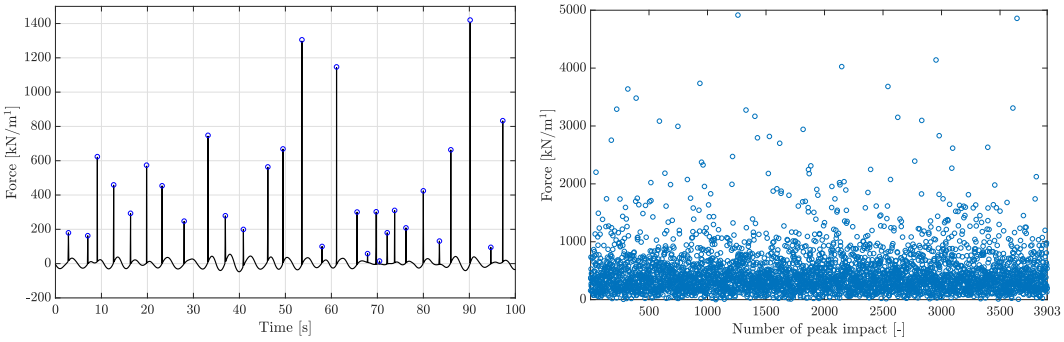

Fig. 12. Wave force distributed over the gate width for a random one minute storm interval (left) and all peak pressures that occur within the entire 4 h storm simulation.

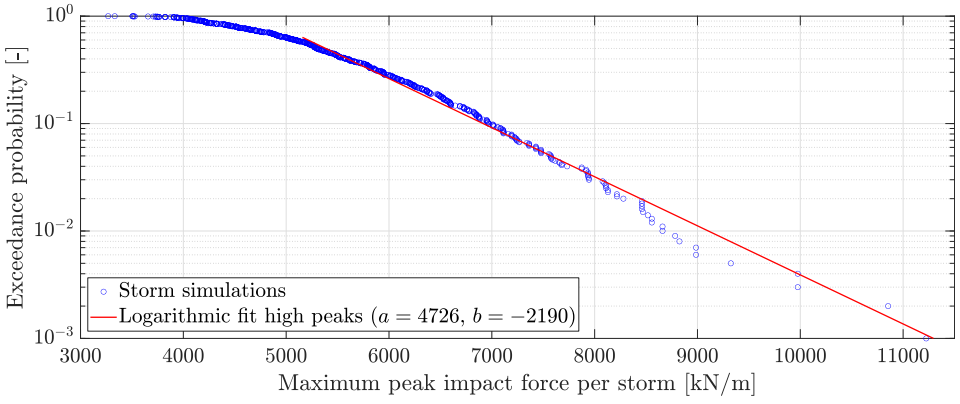

Fig. 13. Exceedance probability of the maximum depth-integrated peak pressure in a single storm with a duration of 4 h based on the 1000 simulations.

6.5. Accuracy of the Monte Carlo simulation

The accuracy of the performed simulation is now discussed. Generally, the coefficient of variation (relative error) ϵ of a Monte Carlo analysis resulting can be estimated by Jonkman et al. (2016):

$$\epsilon = \frac{1}{\sqrt{N\, p_f}} \tag{51}$$

in which N is the number of simulations and p_f the required failure probability. For the failure probability and number of simulations in our case this leads to an approximate coefficient of variation of 10%.

This estimate relies on the assumption that the outcome of the Monte Carlo simulation is binomially distributed. This is generally the case when the underlying stochastic variables are well behaved, also interpreted as slowly varying. It is argued that this is true for the stochastic variables considered in this case study. The correction factor and impulse duration are normally distributed and have a direct linear relation with the peak impact force of the wave impacts. The random-phase amplitude model is known to result in a smooth Rayleigh distribution of the wave height (Holthuijsen, 2007), which in turn is also linearly related to the impact velocity and peak impact force.

Fig. 17 shows that the resulting distribution of the maximum stresses is indeed approximately binomial for the situation regarded in the case study. However, the distribution does show a double peak and is not entirely smooth at its tail. To obtain an additional indication of the robustness of the result, the number of simulations is varied. As shown in Fig. 18, the found probability of failure is relatively stable after 300 simulations at least when compared to the requirement.

This accuracy is therefore expected to be sufficient for this case study. For design, when optimising the design for the required failure probability, a higher number of simulations could be desirable however. Alternatively, sampling techniques exist that can improve the accuracy for a given number of simulations (Jonkman et al., 2016).

In the performed case study the water level was considered to be constant at the level of the overhang. It must be noted that a less smooth result is expected when performing a multivariate probabilistic analyse both including wave heights and water levels. Maximum wave impact forces occur when the water level is equal to the bottom of the overhang, which could possibly be just a small interval compared to the stochastic variation in water levels in some cases. Such an analysis therefore most likely requires a higher number of simulations.

7. Conclusion

A semi-analytical fluid–structure interaction (FSI) model has been developed to accurately predict the dynamic behaviour of flood gates

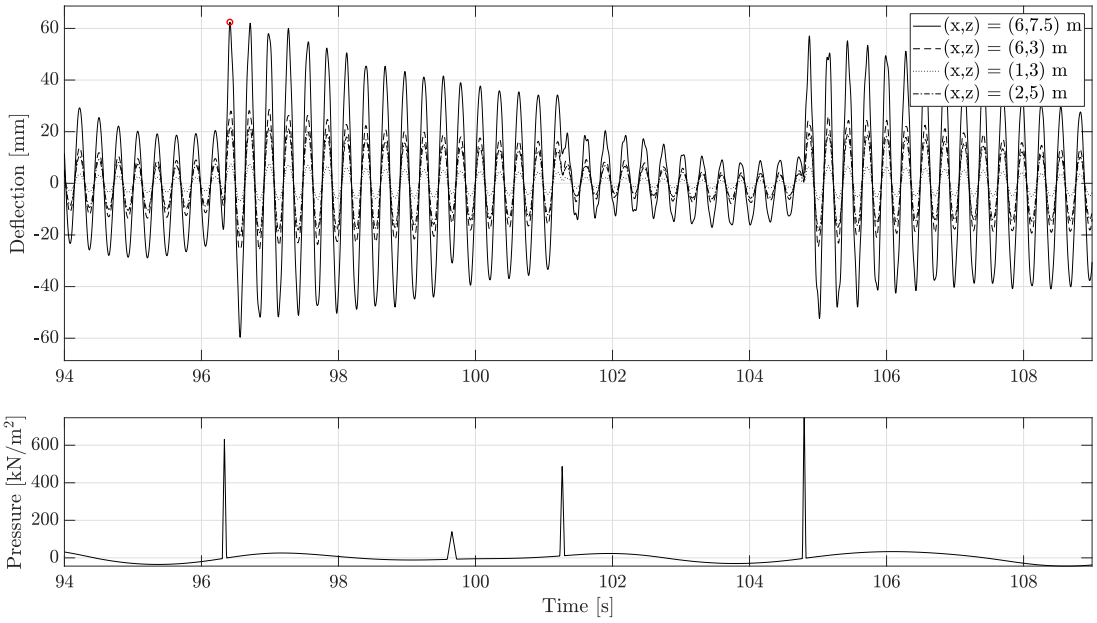

Fig. 14. The displacement response of the gate for several wave impacts within a storm simulation.

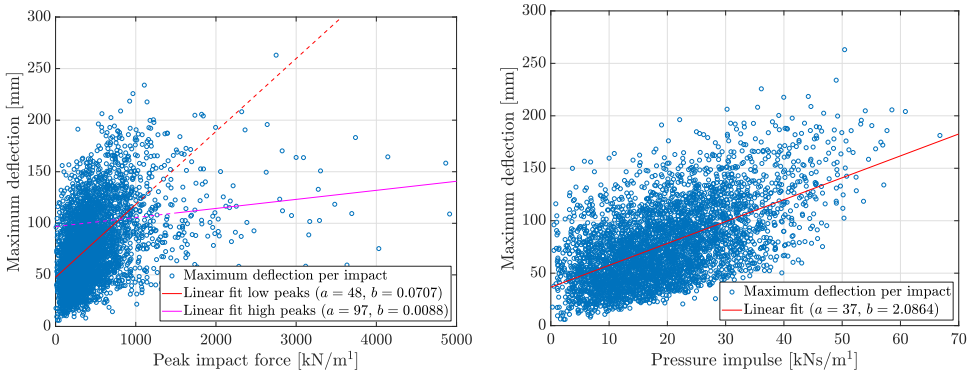

Fig. 15. Correlation between the maximum local deflection of the gate and the peak impact force (left) and the pressure impulse (right) for all wave impacts within a single storm simulation.

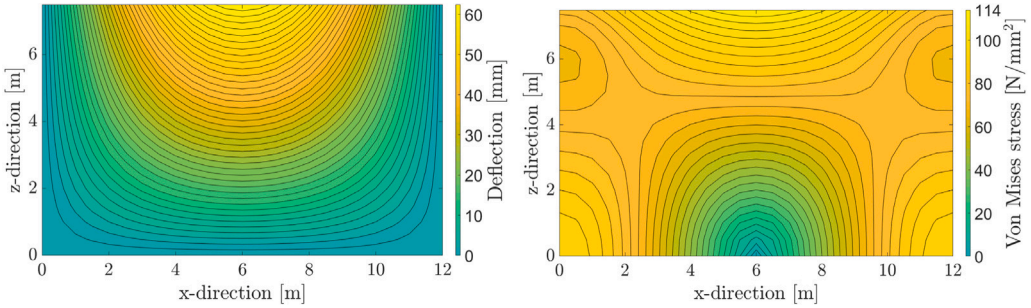

Fig. 16. Deflection and stress at the surface of the plate at a local maximum response ($t = 96.4$ s) to a wave impact.

in complex fluid domains. It includes the two way fluid–structure interaction in a computationally efficient manner. The situation of impact loads on an overhanging structure in front of the gate is considered, which can for example be the case with culverts or bridge decks on top of discharge sluices. The FSI model is an extension of a previous model (Tieleman et al., 2019a), which makes it applicable to the types dewatering sluices studied. For this purpose, the presence of the overhang that causes the confined-wave impacts and a new wide domain outside the channel have been added. The method of solution is based on a mode matching technique of the structure and fluid. The effect of surface waves compressibility of the fluid on both sides of the gate is included in the model. The performance of the developed fluid–structure interaction model has been compared to conventional FE software, showing accurate results with much better computational efficiency.

A recently validated approach is employed to predict the wave impact loads on the gate, making use of different theories are applied to predict the quasi-steady pulsating and impulsive impact part of the

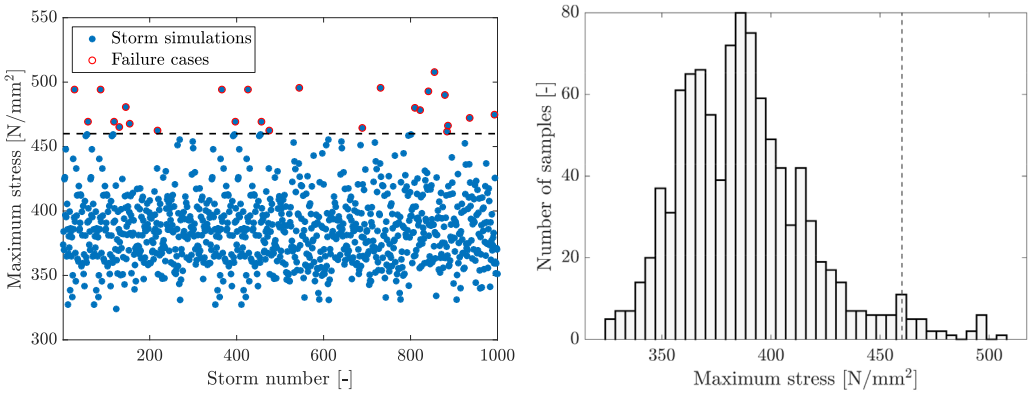

Fig. 17. Maximum stress found in each of the 1000 storm simulations compared to the deterministic value of the yield strength (left) and the number of samples per maximum stress interval (right).

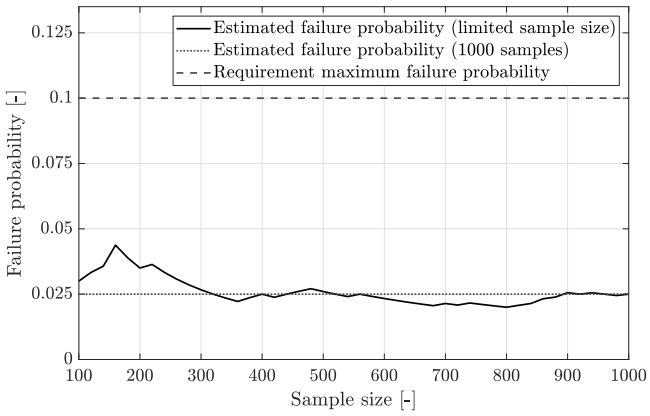

Fig. 18. The probability of failure found for an increasing number of simulations.

wave load. For the impact part, pressure impulse theory is applied, which has shown a better theoretical predictability than peak pressures. Employing this method, avoids the necessity for time-consuming and costly experiments for every new situation. The combination of the relatively new FSI model and the analytical formulation to obtain the impulse of the confined-wave impacts was not applied before.

The computational efficiency of the developed models allows for a large number of simulations. This makes it possible for the first time to perform probabilistic evaluations or predict the response to every single wave over the lifetime of the structure without doing concessions on the accuracy of the physical modelling of the involved fluid–structure interaction processes, which is a novelty within the field of hydraulic structures. A probabilistic approach has been presented to demonstrate this use, explicitly quantifying the failure probability of a flood gate subjected to wave impacts for a given design storm. Within this approach, a large number of storms is simulated, each having a duration of several hours and involving a few thousand wave impacts. The free surface elevation, wave impact duration and impulse correction factor are considered stochastically. The response of the flood gate is investigated for each storm simulation. Predicting the response of the flood gate to each storm simulation using existing time-domain FE models would be a computationally impossible mission.

The probabilistic approach and developed gate-fluid and wave load model are applied to a case study inspired by the situation of the Afsluitdijk, demonstrating their applicability as an advanced design method. For the case study, vibrations of the gate did not damp out between wave impacts. The sequence and exact moment of wave impacts therefore influence the maximum response of the flood gate. This effect is not included in more conventional design methods, but is captured well within the presented probabilistic approach.

Furthermore, results show that the pressure impulse is not only better predictable than the peak pressure when regarding the wave impact load, but also the response of the flood gate is more strongly correlated to the pressure impulse. This further motivates the use of pressure impulse theory as the governing load parameters for wave impacts on these particular type of structures, where now the peak pressures are generally considered in design practice.

Finally, it is recommended to include the water level variation during the course of a storm within the presented probabilistic approach. This variation is also of interest when applying the developed model for fatigue assessments, explicitly predicting stress cycles for a large number of storms and wave loads.

CRediT authorship contribution statement

O.C. Tieleman: Conceptualization, Methodology, Software, Validation, Formal analysis, Writing – original draft, Visualization. **B. Hofland:** Conceptualization, Methodology, Writing – review & editing, Project administration. **A. Tsouvalas:** Conceptualization, Methodology, Writing – review & editing. **E. de Almeida:** Conceptualization, Methodology, Writing – review & editing. **S.N. Jonkman:** Conceptualization, Methodology, Writing – review & editing.

Declaration of competing interest

The authors declare that they have no known competing financial interests or personal relationships that could have appeared to influence the work reported in this paper.

Acknowledgements

This research was supported by NWO, Netherlands grant ALWTW.2016.041.

References

de Almeida, E., Hofland, B., 2020. Experimental observations on impact velocity and entrapped air for standing wave impacts on vertical hydraulic structures with overhangs. J. Mar. Sci. Eng. 8 (11), 857.

Bagnold, R.A., 1939. Interim report on wave-pressure research. In: J. Inst. Civil Eng.. 12, (7), Institution of Civil Engineers, pp. 202–226. http://dx.doi.org/10.1680/ijoti.1939.14539.

Chen, X., Hofland, B., Molenaar, W., Capel, A., Van Gent, M.R., 2019. Use of impulses to determine the reaction force of a hydraulic structure with an overhang due to wave impact. Coast. Eng. 147, 75–88.

COMSOL Inc, 2018. COMSOL Multiphysics Reference Manual, version 5.3. Technical Report, URL: https://www.comsol.com.

Cuomo, G., 2007. Wave impacts on vertical seawalls and caisson breakwaters. In: PIANC Magazine "on Course", Vol. 127.

De Almeida, E., Hofland, B., 2020. Validation of pressure-impulse theory for standing wave impact loading on vertical hydraulic structures with short overhangs. Coast. Eng. 159 (March), 103702.

De Almeida, E., Hofland, B., Jonkman, S., 2019. Wave Impact Pressure-Impulse on Vertical Structures with Overhangs, Vol. 9. (1974), pp. 86–96.

Hasselmann, K., 1973. Measurements of Wind-Wave Growth and Swell Decay During the Joint North Sea Wave Project (JONSWAP). Technical Report, Deutches Hydrographisches Institut.

Hofland, B., Kaminski, M., Wolters, G., 2011. Large scale wave impacts on a vertical wall. Coast. Eng. Proc. 1 (32), 15.

Holthuijsen, L.H., 2007. Waves in Oceanic and Coastal Waters, Vol. 1.

Jensen, F.B., Kuperman, W.A., Porter, M.B., Schmidt, H., 2011. Computational Ocean Acoustics. Springer New York, New York, NY, URL: http://link.springer.com/10.1007/978-1-4419-8678-8.

Jonkman, S.N., Steenbergen, R.D.J.M., Morales-Nápoles, O., Vrouwenvelder, A.C.W.M., Vrijling, J.K., 2016. Probabilistic Design: Risk and Reliability Analysis in Civil Engineering. Technical Report, Delft University of Technology.

Kisacik, D., Troch, P., Van Bogaert, P., Caspeele, R., 2014. Investigation of uplift impact forces on a vertical wall with an overhanging horizontal cantilever slab. Coast. Eng. 90, 12–22.

Kolkman, P.A., Jongeling, T.H.G., 2007a. Dynamic Behaviour of Hydraulic Structures - Part B. WL | Delft Hydraulics.

Kolkman, P.A., Jongeling, T.H.G., 2007b. Dynamic Behaviour of Hydraulic Structures - Part a. WL | Delft Hydraulics.

Leblond, C., Sigrist, J., Auvity, B., Peerhossaini, H., 2009. A semi-analytical approach to the study of an elastic circular cylinder confined in a cylindrical fluid domain subjected to small-amplitude transient motions. J. Fluids Struct. 25 (1), 134–154.

Leissa, A.W., 1969. Vibration of Plates. NASA; United States, Washington, D.C..

Ramkema, C., 1978. A model law for wave impacts on coastal structures. Coast. Eng. Proc. 16 (Figure 7), 2308–2327.

Rijkswaterstaat, 2020. Project overview afsluitdijk. URL: https://www.rijkswaterstaat.nl/water/projectenoverzicht/afsluitdijk.

Schmidt, H., Tango, G., 1986. Efficient global matrix approach to the computation of synthetic seismograms. Geophys. J. Int. 84 (2), 331–359.

Tadjbakhsh, I., Keller, J.B., 1960. Standing surface waves of finite amplitude. J. Fluid Mech. 8 (03), 442.

Tieleman, O.C., 2016. The dynamic behaviour of pump gates in the Afsluitdijk. Technical Report, Delft University of Technology.

Tieleman, O.C., Hofland, B., Jonkman, S.N., 2018. Bending vibrations of the afsluitdijk gates subjected to wave impacts: A comparison of two design methods. In: Proceedings of the 34th PIANC World Congress.

Tieleman, O.C., Tsouvalas, A., Hofland, B., 2019b. Effect of compressibility and surface waves on the hydrodynamic pressures for a vertical flood gate. In: Proceedings of the Twenty-Ninth (2019) International Ocean and Polar Engineering Conference. pp. 3349–3356.

Tieleman, O.C., Tsouvalas, A., Hofland, B., Peng, Y., Jonkman, S., 2019a. A three dimensional semi-analytical model for the prediction of gate vibrations immersed in fluid. Mar. Struct. 65, 134–153.

Tsouvalas, A., van Dalen, K.N., Metrikine, A.V., 2015. The significance of the evanescent spectrum in structure-waveguide interaction problems. J. Acoust. Soc. Am. 138 (4), 2574–2588.

Tsouvalas, A., Metrikine, A., 2014. A three-dimensional vibroacoustic model for the prediction of underwater noise from offshore pile driving. J. Sound Vib. 333 (8), 2283–2311.

Tsouvalas, A., Metrikine, A., 2016. Noise reduction by the application of an air-bubble curtain in offshore pile driving. J. Sound Vib. 371, 150–170.

Tsouvalas, A., Molenkamp, T., Canny, K., Kroon, D., Versluis, M., Peng, Y., Metrikine, A., 2020. A mode matching technique for the seismic response of liquid storage tanks including soil-structure interaction. (June), pp. 1–14. http://dx.doi.org/10.47964/1120.9001.18621, URL: https://www.easdprocedia.org/conferences/easd-conferences/eurodyn-2020/9001.

Vrijling, J., 2001. Probabilistic design of water defense systems in The Netherlands. Reliab. Eng. Syst. Saf. 74 (3), 337–344.

van der Wal, R.J., de Boer, G., 2004. Downtime analysis techniques for complex offshore and dredging operations. In: 23rd International Conference on Offshore Mechanics and Arctic Engineering, Vol. 2. ASMEDC, pp. 93–101. http://dx.doi.org/10.1115/OMAE2004-51113, URL: https://asmedigitalcollection.asme.org/OMAE/proceedings/OMAE2004/37440/93/300213.

Wood, D., Peregrine, D., 1997. Wave impact beneath a horizontal surface. In: Coastal Engineering 1996. American Society of Civil Engineers, New York, NY, pp. 2573–2583. http://dx.doi.org/10.1061/9780784402429.199, URL: http://ascelibrary.org/doi/10.1061/9780784402429.199.

Zheng, X., Gao, S., Huang, Y., 2020. Cross-mode couplings for the fatigue damage evaluation of trimodal Gaussian processes. Ocean Eng. 202 (January), 107177.